

# Characterizing chemical abundance ratios in extremely metal-poor star-forming galaxies in DESI EDR

I. A. Zinchenko<sup>1,2</sup>, M. Sobolenko<sup>2</sup>, J. M. Vílchez<sup>3</sup>, and C. Kehrig<sup>3</sup>

<sup>1</sup> Faculty of Physics, Ludwig-Maximilians-Universität, Scheinerstr. 1, 81679 Munich, Germany

<sup>2</sup> Main Astronomical Observatory, National Academy of Sciences of Ukraine, 27 Akademika Zabolotnoho St., 03143, Kyiv, Ukraine

<sup>3</sup> Instituto de Astrofísica de Andalucía (CSIC), Apartado 3004, 18080 Granada, Spain

August 9, 2024

## ABSTRACT

We present a search for galaxies in the local Universe with extremely low oxygen abundance, that is, more than 25 times lower than solar, which corresponds to  $12 + \log(\text{O/H}) < 7.3$ . To determine the oxygen abundance, we apply the direct  $T_e$  method for objects where the  $[\text{O III}]\lambda 4363$  line is detected. We identified 21 extremely metal-poor galaxies in the early data release of the Dark Energy Spectroscopic Instrument (DESI EDR), for some of which we also derived N/O, Ne/O, Ar/O, and S/O ratios. We find that many DESI galaxies with extremely low oxygen abundance exhibit a higher N/O ratio in comparison to the reference low-metallicity sample collected from the literature. We suggest that the elevation in N/O ratio may be explained by a contamination with metal-rich gas caused by gas inflow or a merger event. Moreover, contrary to some recent studies, we find that Ar/O and S/O ratios are enhanced as well, while the Ne/O ratio does not show such elevation. One of the galaxies, J0713+5608, has a remarkably low oxygen abundance of  $6.978 \pm 0.095$  dex. This measurement aligns with the lowest known oxygen abundances in galaxies to date. Given the relatively high uncertainty, this galaxy may have the lowest oxygen abundance ever found. Additionally, J0713+5608 exhibited an enhanced N/O ratio compared to the typical N/O ratio observed in metal-poor galaxies within the local Universe.

**Key words.** galaxies: abundances – galaxies: evolution – H II regions

## 1. Introduction

Extremely metal-poor galaxies are relatively uncommon objects in the local Universe, yet they serve as excellent laboratories for the examination of physical conditions and processes in the primeval Universe and during the epoch of reionization. Consequently, investigating these galaxies holds significant importance for advancing our understanding of the early stages of galaxy evolution.

Several such galaxies have been identified in the local Universe through various studies. Since the confirmation of an extremely low oxygen abundance in the blue compact dwarf (BCD) galaxy IZw18, namely of about  $12 + \log(\text{O/H}) = 7.11$  (see, e.g., Izotov & Thuan 1998a; Kehrig et al. 2016), efforts to discover galaxies with even lower metallicity have been undertaken. For instance, Skillman et al. (2013) measured the oxygen abundance in the H II region of the dwarf galaxy Leo P, finding  $7.17 \pm 0.04$ , while Hsyu et al. (2017) derived an oxygen abundance of  $7.13 \pm 0.08$  dex for the BCD galaxy Little Cub. The BCD galaxy AGC198691 was found to possess a lower oxygen abundance of  $7.02 \pm 0.03$  dex by Hirschauer et al. (2016), or  $7.06 \pm 0.03$  dex in a more recent study by Aver et al. (2022). Similar oxygen abundances ( $12 + \log(\text{O/H}) = 7.035 \pm 0.026$ ) were observed in J1234+3901 by Izotov et al. (2019), in J2229+2725 ( $12 + \log(\text{O/H}) = 7.085 \pm 0.031$ ) by Izotov et al. (2021), and in J2229+2725 ( $12 + \log(\text{O/H}) = 7.085 \pm 0.031$ ) by Izotov et al. (2024).

To date, several galaxies have been reported with oxygen abundances slightly below  $12 + \log(\text{O/H}) = 7.0$ . Annibali et al. (2019) determined a value of  $6.96 \pm 0.09$  dex in one of the H II regions in the dwarf irregular galaxy DDO 68. J0811+4730, with

$12 + \log(\text{O/H}) = 6.98 \pm 0.02$ , was identified by Izotov et al. (2018). Kojima et al. (2020) reported an even lower oxygen abundance of  $6.90 \pm 0.03$  dex for HSC J1631+4426. However, Thuan et al. (2022) reobserved this galaxy with the Large Binocular Telescope (LBT) and determined a significantly higher metallicity of  $12 + \log(\text{O/H}) = 7.14 \pm 0.03$ .

In the present work, we aim to search for extremely metal-poor galaxies ( $12 + \log(\text{O/H}) < 7.3$ ) in the local Universe ( $z < 0.5$ ) in the early data release of the Dark Energy Spectroscopic Instrument (DESI EDR; DESI Collaboration et al. 2023) using the direct  $T_e$  method and explore abundances of O, N, Ne, Ar, S, and Fe, the emission lines of which are available in the optical spectrum. The paper is organized as follows. In Sect. 2 we provide a detailed description of the data used for further analysis. Section 3 describes the method of determination of chemical abundances and other physical properties. In Sect. 4 we discuss the obtained sample of extremely metal-poor galaxies. In Sect. 5 we describe the galaxy with the lowest oxygen abundance. Finally, Sect. 6 presents a summary of our main findings.

## 2. Data

For this study, we analyzed a subset of galaxies from the DESI EDR survey (DESI Collaboration et al. 2023). The DESI EDR includes spectra for 1.8 million distinct targets observed during Survey Validation, commissioning, and special tiles, spanning December 2020 to June 2021.

We analyzed 666773 DESI spectra of galaxies with redshifts of less than 0.5, where  $\text{H}\alpha$  falls within the DESI wavelength range. From the analysis point of view, DESI spectra do not show significant differences with respect to the other

**Table 1.** General characteristics of our sample of galaxies from the DESI EDR

Name	Target ID	RA deg	DEC deg	Redshift	$\text{mag}_g$ mag	$\text{mag}_r$ mag	$M_g$ mag	Exptime s
J1143-0139	39627745398883762	175.815730	-1.651681	0.1445	20.65	20.45	-18.31	4215
J0941+3209	39628526860634476	145.296859	32.156355	0.0213	19.79	19.67	-15.01	5623
J1333+3326	39632951142518497	203.301564	33.438166	0.1253	23.05	23.02	-15.60	617
J0224-0328	39627700792463174	36.141673	-3.474988	0.1770	23.89	23.75	-15.51	10800
J1212-0044	39627769679712162	183.167657	-0.748498	0.0404	23.17	23.84	-13.03	10581
J1003+0123	39627823496826637	150.926393	1.385053	0.0998	23.68	23.80	-14.48	13500
J1225+3151	39628517175986127	186.274146	31.862207	0.0443	23.35	23.55	-13.04	2991
J0847+3257	39632940019221902	131.901191	32.953882	0.1418	23.53	23.65	-15.39	4555
J0901+3336	39632950190410845	135.403924	33.603166	0.1162	22.05	22.06	-16.44	5508
J0651+3843	39633052476903702	102.917068	38.733027	0.0662	23.23	23.42	-14.03	9184
J0713+5608	39633338331299912	108.360899	56.142043	0.0389	22.63	22.51	-13.48	13500
J0923+6451	39633440282250119	140.880315	64.853146	0.0054	20.71	20.48	-11.13	9000
J1505+3146	39628517750604871	226.399556	31.777634	0.0543	20.51	20.57	-16.32	2066
J1802+6439	39633441217579195	270.597146	64.656143	0.0494	19.20	19.00	-17.43	285
J1434-0055	39627764235503713	218.584632	-0.923267	0.1370	22.74	22.44	-16.11	1566
J1001+0241	39627853687427435	150.439479	2.691775	0.2192	23.10	22.34	-16.77	2881
J1257+2348	39628346086134793	194.450750	23.810648	0.0887	23.17	23.12	-14.73	2653
J1256+2433	39628362649440128	194.170086	24.551167	0.0488	21.65	21.83	-14.96	870
J1301+2505	39628373655292169	195.266315	25.099504	0.0257	20.75	20.71	-14.46	870
J1651+3356	39632961900904930	252.865044	33.936124	0.1127	23.88	25.26	-14.54	842
J1536+4346	39633145200381558	234.133969	43.767690	0.4662	23.80	23.82	-17.70	1499

**Table 2.** Electron densities, [O III] temperatures  $t_3$ , and element abundances in the DESI EDR galaxies

Target ID	$n_e(\text{[S II]})$ $\text{cm}^{-3}$	$n_e(\text{[O II]})$ $\text{cm}^{-3}$	$t_3$ $10^4 \text{K}$	12+log(O/H) dex	12+log(N/H) dex	12+log(Ne/H) dex	12+log(Ar/H) dex	12+log(S/H) dex
J1143-0139	265±212	123±112	2.24±0.14	7.219±0.041	5.784±0.093	6.459±0.066	4.596±0.077	—
J0941+3209	<100	<100	2.63±0.55	7.145±0.095	5.830±0.121	6.282±0.163	—	5.617±0.070
J1333+3326	—	<100	2.78±0.48	7.250±0.093	—	—	—	—
J0224-0328	—	<100	2.13±0.30	7.286±0.096	—	6.607±0.140	—	—
J1212-0044	<100	79±112	2.22±0.35	7.235±0.088	5.679±0.150	6.434±0.142	4.923±0.119	5.640±0.079
J1003+0123	—	205±172	2.96±0.57	7.111±0.079	—	6.295±0.127	—	—
J1225+3151	<100	<100	2.31±0.30	7.260±0.085	—	6.592±0.113	5.041±0.134	5.920±0.080
J0847+3257	—	140±237	2.30±0.30	7.268±0.086	—	6.528±0.130	—	—
J0901+3336	<100	<100	2.29±0.15	7.290±0.038	—	6.555±0.070	—	—
J0651+3843	217±237	<100	2.44±0.43	7.232±0.095	6.079±0.153	6.488±0.132	—	5.822±0.122
J0713+5608	124±234	70±65	2.73±0.48	6.978±0.095	5.864±0.131	6.125±0.155	4.603±0.161	—
J0923+6451	42±60	18±17	2.06±0.13	7.170±0.051	5.898±0.071	6.471±0.071	4.899±0.061	5.755±0.037
J1505+3146	<100	272±212	2.37±0.10	7.139±0.029	—	6.450±0.044	4.464±0.097	5.397±0.033
J1802+6439	70±112	172±112	2.80±0.47	7.208±0.071	6.022±0.104	6.526±0.123	—	—
J1434-0055	—	165±212	2.53±0.34	7.249±0.084	—	6.525±0.104	—	—
J1001+0241	1248±1424	<100	2.34±0.12	7.168±0.038	—	6.486±0.048	4.934±0.084	—
J1257+2348	—	117±112	2.89±0.47	7.229±0.076	—	6.526±0.113	—	—
J1256+2433	37±65	<100	2.35±0.16	7.281±0.044	5.916±0.101	6.547±0.060	5.094±0.078	5.772±0.037
J1301+2505	<100	28±34	2.22±0.31	7.116±0.078	—	6.211±0.127	4.786±0.119	5.482±0.062
J1651+3356	—	221±237	2.44±0.42	7.288±0.099	—	6.670±0.123	—	—
J1536+4346	—	392±399	2.53±0.36	7.238±0.081	—	6.303±0.134	—	—

optical spectroscopic surveys (e.g., the Sloan Digital Sky Survey (SDSS), the Calar Alto Legacy Integral Field Area Survey (CALIFA), Mapping Nearby Galaxies at APO (MaNGA)), as they have compatible spatial and spectral resolutions and wavelength ranges. Therefore, for analysis of DESI spectra, we employed the methodology that has been applied in our previous studies of the multi-object spectroscopy (MOS) and integral field units (IFU) spectra outlined in, for example, [Zinchenko et al. \(2016, 2021\)](#) and [Lara-López et al. \(2023\)](#). In essence, the stellar background was fitted using the public version of the STARLIGHT code ([Cid Fernandes et al. 2005; Mateus et al. 2006; Asari et al. 2007](#)), customized for parallel processing of

individual spectra. Simple stellar population (SSP) spectra from the evolutionary synthesis models by [Bruzual & Charlot \(2003\)](#) were used to fit the stellar spectra and were subsequently subtracted from the observed spectrum to derive a pure gas spectrum.

We used our ELF3D code for emission line fitting, which is able to fit complex line profiles such as blends or profiles with broad and narrow components. The recent ELF3D version is based on the LMfit library and shared-memory parallelization. This approach reduces the number of dependencies and improves the portability of the code. In this work, we fit each emission line with a single Gaussian profile. A full list of mea-

**Table 3.** Ion abundances in the DESI EDR galaxies

Name	O <sup>+</sup> /H	O <sup>2+</sup> /H	N <sup>+</sup> /H	Ne <sup>2+</sup> /H	Ar <sup>2+</sup> /H	S <sup>+</sup> /H	S <sup>2+</sup> /H
J1143-0139	6.570±0.060	7.109±0.051	5.146±0.093	6.420±0.066	4.543±0.077	4.870±0.043	—
J0941+3209	6.836±0.143	6.851±0.115	5.519±0.121	6.201±0.163	—	5.266±0.092	5.443±0.096
J1333+3326	6.422±0.151	7.181±0.104	—	—	—	—	—
J0224-0328	6.649±0.128	7.172±0.115	—	6.566±0.140	—	—	—
J1212-0044	6.739±0.133	7.067±0.109	5.183±0.150	6.380±0.142	4.889±0.119	5.072±0.082	5.472±0.103
J1003+0123	6.638±0.130	6.933±0.095	—	6.237±0.127	—	—	—
J1225+3151	6.349±0.115	7.203±0.095	—	6.570±0.113	4.933±0.134	4.789±0.097	5.593±0.091
J0847+3257	6.307±0.128	7.218±0.094	—	6.508±0.130	—	—	—
J0901+3336	6.601±0.059	7.190±0.045	—	6.519±0.070	—	4.926±0.057	—
J0651+3843	6.401±0.135	7.162±0.107	5.275±0.153	6.462±0.132	—	4.883±0.105	5.523±0.145
J0713+5608	6.468±0.147	6.817±0.115	5.356±0.131	6.072±0.155	4.567±0.161	4.960±0.091	—
J0923+6451	6.511±0.071	7.063±0.061	5.251±0.071	6.432±0.071	4.846±0.061	5.020±0.045	5.535±0.046
J1505+3146	6.300±0.044	7.071±0.033	—	6.424±0.044	4.374±0.097	4.646±0.032	5.033±0.045
J1802+6439	6.819±0.112	6.981±0.086	5.629±0.104	6.455±0.123	—	5.378±0.081	—
J1434-0055	6.404±0.117	7.182±0.094	—	6.499±0.104	—	—	—
J1001+0241	5.809±0.069	7.148±0.039	—	6.477±0.048	4.630±0.084	4.316±0.087	—
J1257+2348	6.554±0.127	7.126±0.089	—	6.489±0.113	—	—	—
J1256+2433	6.547±0.057	7.192±0.052	5.201±0.101	6.514±0.060	5.028±0.078	5.064±0.044	5.483±0.048
J1301+2505	6.745±0.114	6.875±0.099	—	6.138±0.127	4.755±0.119	4.993±0.076	5.350±0.081
J1651+3356	6.269±0.141	7.245±0.108	—	6.653±0.123	—	—	—
J1536+4346	6.336±0.129	7.180±0.089	—	6.280±0.134	—	—	—

sured emission lines can be found in Table B.1. A comparison of measured fluxes with the ones obtained from SDSS spectra in the MPA/JHU catalog is discussed in Appendix A and Fig. A.1.

Then, the line fluxes were corrected for interstellar reddening following the extinction curve from Fitzpatrick (1999), assuming a Balmer line ratio for high electron temperatures ( $T_e \sim 20000$  K),  $H\alpha/H\beta = 2.75$ . In cases where the measured value of  $H\alpha/H\beta$  was less than 2.75, the reddening correction was set to zero.

To select spectra of star-forming regions, we applied the  $\log([O\text{ III}]\lambda 5007/H\beta) - \log([N\text{ II}]\lambda 6584/H\alpha)$  diagram (Baldwin et al. 1981). Consequently, we selected spectra where [O III] $\lambda 5007$ , H $\beta$ , and H $\alpha$  emission lines were detected with a signal-to-noise ratio (S/N) exceeding 3. No S/N constraint was imposed on [N II] $\lambda 6584$ , because this line is anticipated to exhibit very low flux in H II regions with extremely low metallicity (e.g., Denicoló et al. 2002). When the S/N of [N II] $\lambda 6584$  fell below 3, the spectrum was classified as belonging to a star-forming region. In instances of detected [N II] $\lambda 6584$ , we selected only spectra where the primary ionization source was identified as massive stars, guided by the dividing line proposed by Kauffmann et al. (2003). Additionally, we imposed  $S/N > 3$  for [O II] $\lambda\lambda 3727,3729$  lines to enable estimation of the chemical abundance of the O<sup>+</sup> ion.

The relation between the auroral line [O III] $\lambda 4363$  and the electron temperature is significantly nonlinear and becomes flatter at high electron temperatures, which corresponds to the low metallicity. Therefore, small uncertainties in [O III] $\lambda 4363$  flux lead to high uncertainties in the electron temperature, and objects with slightly overestimated [O III] $\lambda 4363$  flux will have underestimated metallicity. To minimize this effect and the probability of the spurious detection of the [O III] $\lambda 4363$  line, we adopted a slightly higher detection threshold of  $S/N > 4$  for the auroral line [O III] $\lambda 4363$ . It is interesting to note that applying this criterion to the [O III] $\lambda 4363$  line leads to a final sample of galaxies (described in Sect. 4) with  $S/N > 5$  for all [O II] $\lambda\lambda 3727,3729$ , H $\beta$ , [O III] $\lambda 5007$ , and H $\alpha$  lines.

### 3. Determination of the chemical abundances, electron densities, and temperatures

In this section, we describe our methodology for determining electron densities ( $n_e$ ) and temperatures ( $T_e$ ) along with chemical abundances. Computations were executed using PyNeb code version 1.1.18 (Luridiana et al. 2015) with default atomic data PYNEB\_23\_01.

The spectral resolution of DESI spectra allows robust measurements of each line in the [O II] $\lambda\lambda 3727,3729$  doublet. Consequently, we derived  $n_e$  from the [O II] $\lambda 3727$ /[O II] $\lambda 3729$  and [S II] $\lambda 6717$ /[S II] $\lambda 6731$  diagnostic line ratios. The diagnostic line ratios of both O II and S II doublets consistently indicate a low-density regime ( $n_e < 300$  cm<sup>-3</sup>) for all objects in our sample. Due to substantial uncertainty at low densities, the computed  $n_e$  values were not used to determine  $T_e$  or chemical abundances. Instead, a fixed value of  $n_e = 100$  cm<sup>-3</sup> was assumed, because its effect is negligible in the calculation of final ionic abundances.

For all galaxies within our sample,  $T_e$  values were directly derived using the [O III] $\lambda 4363$  auroral line. Following the approach described by Pérez-Montero (2017) and Garnett (1992), we adopted a three-zone temperature model with electron temperatures  $t_h$ ,  $t_m$ , and  $t_l$  in the inner, intermediate, and outer zones, respectively, which establishes a link between  $T_e$  derived in the [O III] zone and the high-temperature zone:

$$t_h = T_e([O\text{ III}]), \quad (1)$$

and assumes the same  $t_h$  in zones of [Ne III], [Fe III], and [Ar IV]. For other ions, we adopted the following scheme:

$$t_m = T_e([Ar\text{ III}]) = T_e([S\text{ III}]), \quad (2)$$

$$t_l = T_e([O\text{ II}]) = T_e([N\text{ II}]) = T_e([S\text{ II}]). \quad (3)$$

We then derived  $t_m$  from the relation between  $T_e([S\text{ III}])$  and  $T_e([O\text{ III}])$  proposed by Hägele et al. (2006):

$$t_m = 1.19t_h - 0.32, \quad (4)$$

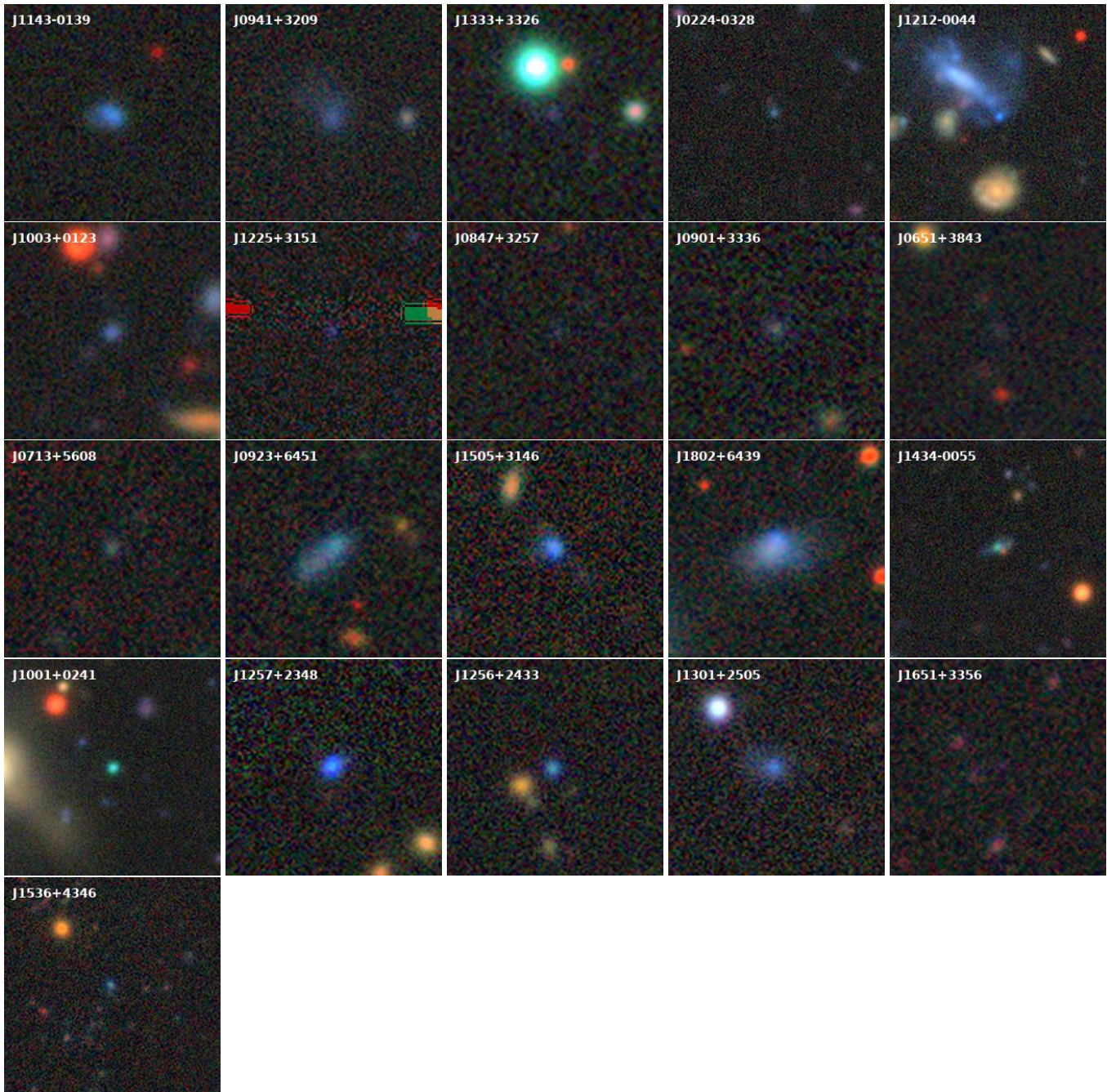


**Fig. 1.** Color composite image of galaxies made using three optical bands (g, r, z) taken from the Legacy Survey DR9 sky map, except for J0224-0328, J1212-0044, J1003+0123, J1434-0055, and J1001+0241, which incorporate an image from Hyper Suprime-Cam (HSC) Subaru Strategic Program DR3. Each image is sized uniformly at 25'' by 25'' centered on the spectral target of all observed objects. North is up and east is left. The image of J1225+3151 has artifacts from a bright star nearby.

and  $t_l$  was obtained from the relation between  $t_l$  and  $t_h$  suggested by [Garnett \(1992\)](#):

$$t_l = 0.7t_h + 0.3. \quad (5)$$

Having determined  $n_e$  and  $T_e$ , we proceeded to derive the abundance of the  $O^+$  ion from the flux of  $[O\text{ II}]\lambda\lambda 3727, 3729$  lines, the abundance of the  $O^{2+}$  ion from  $[O\text{ III}]\lambda\lambda 4959, 5007$  lines, and the total oxygen abundance as the sum of the ionic abundances of  $O^+/H^+$  and  $O^{2+}/H^+$ . This procedure was applied to other ions for which we detected at least one nebular emission line. Then, ionization correction factors (ICFs) from [Izotov et al. \(2006\)](#) were applied to account for the unseen ionization states.

#### 4. Chemical abundances of galaxies with extremely low metallicity

We derived the oxygen abundance using the  $T_e$  method for a sample of galaxies obtained in Sect. 2. From this sample, we selected a final sample of galaxies with  $12+\log(O/H) < 7.3$ , comprising 21 objects. Among them, 7 galaxies were recently reported as extremely metal-poor by [Zou et al. \(2024\)](#), while the metallicity of the other 14 galaxies is measured for the first time. The general characteristics of these 21 selected galaxies are detailed in Table 1, where information obtained from the DESI catalog is presented, including the name, DESI target ID, right ascension (RA) and declination (DEC) coordinates, red-

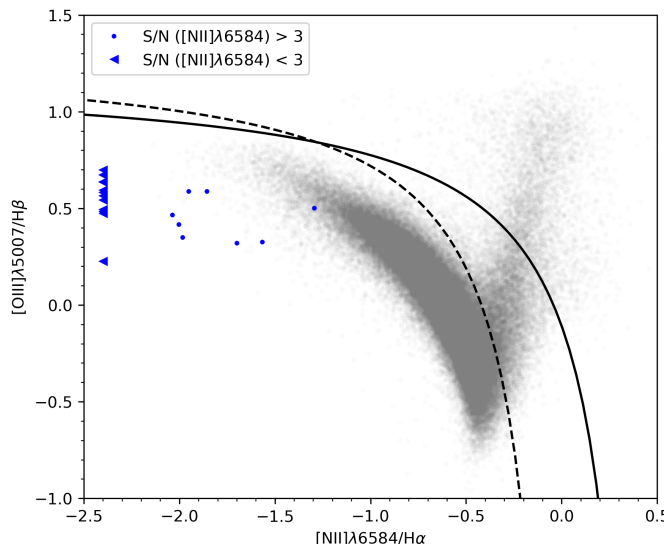


**Fig. 2.** BPT diagram for our sample of extremely low-metallicity galaxies. Blue circles show galaxies with detected  $\text{N II} \lambda 6584$  line, while blue triangles represent galaxies with  $S/N < 3$  in  $\text{N II} \lambda 6584$ . Gray circles represent the entire sample of DESI galaxies with  $z < 0.5$ . The solid line is the theoretical upper limit for star-forming galaxies presented by Kewley et al. (2001). The dashed line is the demarcation line proposed by Kauffmann et al. (2003) as a lower limit for the area of AGNs.

shift, magnitudes in  $g$  and  $r$  bands, and exposure time of the DESI coadd spectrum. Additionally, we estimated the absolute magnitude  $M_g$  based on redshift and  $g$  magnitude. Color composite image cutouts for each galaxy are provided in Fig. 1.

When corresponding emission lines are detected in the spectrum, we derived values of electron density, electron temperature, and chemical abundances of O, N, Ne, Ar, and S, which are summarized in Table 2. Furthermore, Table 3 encapsulates the chemical abundances of the individual ions listed above. Emission line intensities and extinction coefficients  $C(\text{H}\beta)$  used for calculations and equivalent widths of  $\text{H}\beta$  EW( $\text{H}\beta$ ) are reported in the Appendix in Table B.1.

The BPT diagram in Fig. 2 illustrates that our sample of DESI galaxies predominantly occupy the region characterized by high  $[\text{O III}] \lambda 5007/\text{H}\beta$  and low  $[\text{N II}] \lambda 6584/\text{H}\alpha$ , indicative of low-metallicity H II regions. In the luminosity–metallicity diagram in Fig. 3, most galaxies in our sample exhibit metallicities lower than the average values for low- $z$  SDSS galaxies with comparable luminosity (Guseva et al. 2009), aligning more closely with the luminosity–metallicity relation for local metal-poor extreme blue compact galaxies (XBCGs) identified by Kunth & Östlin (2000). According to Kunth & Östlin (2000), XBCGs are 0.5 dex less metal rich at a given luminosity compared to the luminosity–metallicity relation for low-mass galaxies. The large number of galaxies in our sample with properties similar to XBCGs may be explained by the DESI sample selection. The DESI survey was designed to map the large-scale structure over a wide range of look-back times. Therefore, the sample selection favored compact objects, presumably at higher redshifts, rather than H II regions in nearby galaxies.

#### 4.1. N/O abundance ratio

The nitrogen line  $[\text{N II}] \lambda 6584$  has been detected in eight galaxies from our sample, which allowed us to derive the N/O ratio. The top panel of Fig. 4 presents the O/H–N/O diagram for our sample

in comparison with a reference sample of H II regions in nearby galaxies and BCDs/BCGs gathered from the literature (Annibali et al. 2019; Croxall et al. 2016; Haurberg et al. 2015; Nicholls et al. 2014; Toribio San Cipriano et al. 2017; Esteban et al. 2009; Fricke et al. 2001; Garnett et al. 1997; Gonzalez-Delgado et al. 1994; Guseva et al. 2000, 2001, 2003a,b, 2004, 2011; Hägele et al. 2008; Hirschauer et al. 2015; Izotov et al. 1994, 1997; Izotov & Thuan 1998a,b; Izotov et al. 1999, 2001, 2004; Izotov & Thuan 2004; Izotov et al. 2009, 2012; Kehrig et al. 2004; Kennicutt & Skillman 2001; Kniazev et al. 2000; Lee et al. 2005, 2003, 2004; Magrini & Gonçalves 2009; Melbourne et al. 2004; Melnick et al. 1992; Pagel et al. 1992; Peña et al. 2007; Pustilnik et al. 2002, 2003a,b, 2005, 2006; Saviane et al. 2008; Skillman & Kennicutt 1993; Skillman et al. 2003; Stanghellini et al. 2010; Terlevich et al. 1991; Thuan et al. 1995, 1999; van Zee et al. 1997; van Zee 2000; Vílchez & Iglesias-Páramo 2003). This reference sample has been created to collect spectra with reliable measurements of auroral lines published over the last decade. For both samples, we applied the method for determining chemical abundances described in Sect. 3. The red dashed line on the plot denotes the median N/O ratio for the reference sample with an oxygen abundance of less than 8.0 dex. Remarkably, five out of the eight DESI galaxies with extremely low oxygen abundance exhibit a higher N/O ratio than the median value for the reference sample. Their  $1\sigma$  confidence intervals of the N/O ratio lie above the median N/O ratio for the reference sample,  $\log(\text{N}/\text{O}) = -1.48$ , while for the remaining three galaxies, the  $1\sigma$  confidence intervals of the N/O ratio overlap with the median N/O ratio for the reference sample. It should be noted that there is no significant difference between the N/O ratio of BCDs/BCGs and the rest of the reference sample, although we note a mild elevation of the N/O ratio for BCDs/BCGs in a narrow range of the oxygen abundance around 7.2 dex. However, BCDs/BCGs with higher and lower metallicity do not show such a N/O elevation.

Enhancement of the N/O ratio at low metallicity has been reported in several works (e.g., Guseva et al. 2011; Pérez-Montero et al. 2011; Kumari et al. 2018; Zinchenko & Pilyugin 2022). As has been discussed in Pérez-Montero et al. (2011) and Kumari et al. (2018), several mechanisms can be responsible for an enhanced N/O ratio at low metallicity, including a localized nitrogen enrichment of the interstellar medium by WR stars, an inflow of low-metallicity gas, and varying star formation efficiency (SFE). We did not find WR bumps in the spectra of galaxies from our sample. However, since galaxies in our sample are very faint (majority below 22 mag), the S/N ratio in the continuum is quite low for most galaxies. Thus, the presence of WR stars cannot be excluded and additional observations with higher S/N ratios in the background near possible WR bumps are needed to confirm or rule out WR stars as a source of enhanced N/O ratio in these galaxies, though massive WR stars are rare at very low metallicity.

An inflow of low-metallicity gas is very unlikely to result in a measured N/O enhancement in extremely metal-poor galaxies, because it assumes very significant dilution of their O/H from  $12 + \log(\text{O}/\text{H}) \sim 8.2$ , where N/O starts to increase with O/H, down to  $12 + \log(\text{O}/\text{H}) \sim 7.0 - 7.3$ . For example, dilution of  $12 + \log(\text{O}/\text{H}) = 8.2$  gas by 7.0 dex gas to obtain 7.2 dex from 8.2 dex would require about 25 times more inflow gas than the in situ gas with an initial metallicity of 8.2 dex.

In this regard, the opposite scenario is more likely. The inflow of even a small amount of high-metallicity gas, which also has a high N/O ratio, may significantly elevate the N/O ratio. For example, mixing pristine gas of  $12 + \log(\text{O}/\text{H}) = 7.0$  and

$\log(\text{N}/\text{O}) = -1.5$  with only 1% (by atom number) of gas with solar metallicity increases the oxygen abundance by  $\sim 0.2$  dex and  $\text{N}/\text{O}$  by  $\sim 0.3$  dex. Although this scenario has not been widely discussed for extremely low-metallicity galaxies, it has been suggested for more metal-rich galaxies (see, e.g., Schaefer et al. 2020; Zinchenko 2023). Such contamination by metal-rich gas may also explain the scatter in the  $\text{N}/\text{O}$  ratio, as different galaxies have different gas-accretion histories. Discussing the origin of XBCGs, Kunth & Östlin (2000) specify that XBCGs are likely the product of mergers. As can be seen from Fig. 3, most of the galaxies from our sample better fit the luminosity–metallicity relation for XBCGs from Kunth & Östlin (2000) than they do the luminosity–metallicity relation of the SDSS galaxies from Guseva et al. (2009). This fact supports the scenario of inflow of gas with higher metallicity either as an independent event or as a result of merging.

#### 4.2. $\text{Ne}/\text{O}$ , $\text{Ar}/\text{O}$ , and $\text{S}/\text{O}$ abundance ratios

Enhancement of the abundances of other chemical elements in metal-poor star-forming regions also remains an open question. Recent theoretical and observational studies have reported enhanced abundances of some chemical elements in extremely metal-poor star-forming dwarf galaxies, where  $12+\log(\text{O}/\text{H}) \leq 7.69$  (e.g., Takahashi et al. 2018; Kojima et al. 2021; Goswami et al. 2022, 2024). These studies attribute the overabundance of certain chemical elements at very low metallicity to the explosion of very massive stars as pair-instability supernovae (PISNe).

In our sample of 21 DESI galaxies, we derived  $\text{Ne}/\text{O}$  in 20 galaxies,  $\text{Ar}/\text{O}$  in 9 galaxies, and  $\text{S}/\text{O}$  ratios in 8 galaxies. We present these measurements in Fig. 4 following the same approach as for  $\text{N}/\text{O}$ . Similar to previous findings by Kojima et al. (2021) and Arellano-Córdova et al. (2024), we find no enhancement of  $\text{Ne}/\text{O}$  in comparison to the values calculated for low-metallicity galaxies from the literature. However, the majority of galaxies in our sample exhibited increased  $\text{Ar}/\text{O}$  ratios, in contrast to the results reported by Kojima et al. (2021) and Arellano-Córdova et al. (2024). Additionally, we observed an increase in the  $\text{S}/\text{O}$  ratio in most galaxies from our sample.

It is noteworthy that the behavior of the  $\text{S}/\text{O}$  ratio with respect to metallicity has been a longstanding open question. Some studies have indicated that the  $\text{S}/\text{O}$  ratio remains constant with metallicity (e.g., Izotov et al. 2006; Berg et al. 2020; Arellano-Córdova et al. 2024), while others have suggested an increase in the  $\text{S}/\text{O}$  ratio at low metallicity (e.g., Vilchez & Pagel 1988; Dors et al. 2016; Díaz & Zamora 2022). Recently, Goswami et al. (2024) showed that very massive stars undergoing the PISN stage may play a significant role in the chemical enrichment of sulfur in metal-poor galaxies.

#### 5. J0713+5608: galaxy with the lowest oxygen abundance in our sample

One of the galaxies in our sample, J0713+5608, exhibits an exceptionally low oxygen abundance of  $6.978 \pm 0.095$  dex, lower than the oxygen abundance of  $7.11 - 7.17$  dex observed in the well-known extremely metal-poor galaxy I Zw 18 (Izotov & Thuan 1998a; Kehrig et al. 2016). This measurement is compatible with the previously reported lowest oxygen abundance in galaxies, such as DDO 68 (Annibali et al. 2019) and J0811+4730 (Izotov et al. 2018). Despite its minimal oxygen abundance, J0713+5608 demonstrates the highest  $\text{N}/\text{O}$  ratio among our DESI galaxy sample, as depicted in Fig. 4. In contrast,

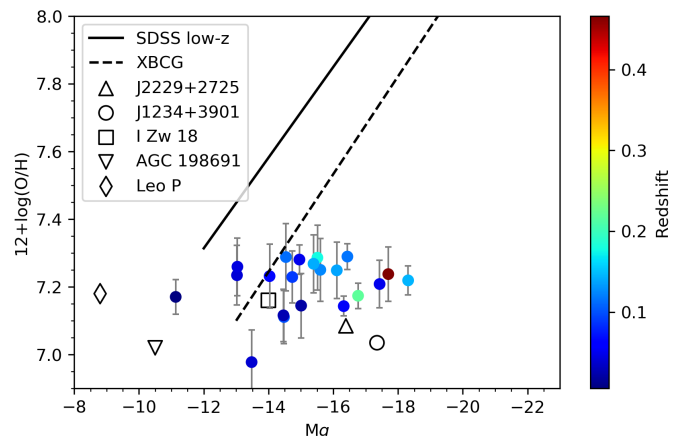


**Fig. 3.** Luminosity–metallicity diagram for our sample of extremely low-metallicity galaxies. Colored circles show galaxies from our sample with color-coded redshift. The solid line is the best fit of the luminosity–metallicity relation for SDSS low-z galaxies obtained by Guseva et al. (2009). The solid line is the best fit of the luminosity–metallicity relation for XBCG obtained by Kunth & Östlin (2000). Open symbols represent galaxies with extremely low metallicity collected from the literature.

its  $\text{Ne}/\text{O}$  and  $\text{Ar}/\text{O}$  ratios align with the typical values observed in our sample and are similar to the median values observed in the reference H II regions.

In the DESI Legacy Survey image, J0713+5608 appears as a faint BCG and occupies a corresponding position on the luminosity–metallicity diagram. Remarkably, with an absolute magnitude of  $M_g = -13.48$ , J0713+5608 lies below the average luminosity–metallicity relation identified by Kunth & Östlin (2000) for XBCGs.

#### 6. Conclusions

We analyzed a subset of galaxies from the DESI EDR survey (DESI Collaboration et al. 2023) to identify extremely metal-poor galaxies. By focusing on DESI spectra with redshifts below 0.5, allowing the inclusion of  $\text{H}\alpha$  within the DESI wavelength range, we performed measurements of the auroral line  $[\text{O III}]\lambda 4363$  and calculated the oxygen abundance using the direct  $T_e$  method.

Among 666773 analyzed galaxies, we find that 21 galaxies exhibit oxygen abundances of below 7.3 dex. Alongside our determination of the oxygen abundance, we derived  $\text{N}/\text{O}$ ,  $\text{Ne}/\text{O}$ ,  $\text{Ar}/\text{O}$ , and  $\text{S}/\text{O}$  ratios for some of these galaxies, which we then compared with corresponding abundance ratios obtained for a reference sample of nearby H II regions and BCD/BCG galaxies. These reference values were derived from a dataset of measured oxygen auroral lines collected from the literature. We find that a fraction of DESI galaxies with extremely low oxygen abundance exhibit higher  $\text{N}/\text{O}$ ,  $\text{Ar}/\text{O}$ , and  $\text{S}/\text{O}$  ratios in comparison to the median values observed within the reference sample. However, it is worth noting that the  $\text{Ne}/\text{O}$  ratio of these extremely metal-poor DESI galaxies does not exhibit a substantial deviation from the  $\text{Ne}/\text{O}$  ratio observed in the reference low-metallicity H II regions and BCD/BCG galaxies. We also suggest that the elevated  $\text{N}/\text{O}$  ratio in some galaxies from our sample can be explained by the scenario of the inflow of gas with higher metallicity either as an independent event or as a result of a merger. However, contributions from WR stars also cannot be excluded.

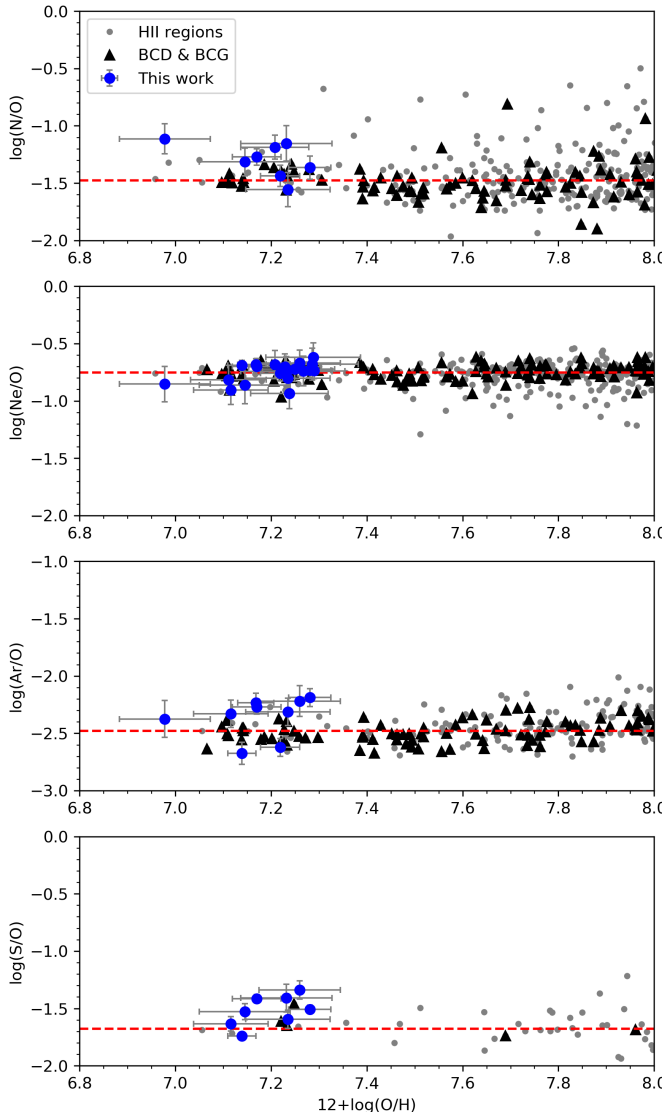


**Fig. 4.** N/O, Ne/O, Ar/O, and S/O ratios with respect to oxygen abundance. Blue circles are our sample of extremely metal-poor galaxies. Gray points and black triangles represent a reference sample of H II regions and BCD/BCG galaxies, respectively, with measured oxygen auroral line collected from the literature. Red dashed lines are medians of N/O, Ne/O, Ar/O, and S/O for the reference H II regions with O/H in the range 7.0 – 8.0 dex.

The galaxy J0713+5608 stands out in our study because of its remarkably low oxygen abundance of  $6.978 \pm 0.095$  dex. This measurement aligns with the lowest known oxygen abundances in galaxies to date. Given the relatively high uncertainty, this galaxy may have the lowest oxygen abundance ever found. Additionally, we found J0713+5608 to exhibit an enhanced N/O ratio compared to the typical N/O ratio observed in metal-poor galaxies within the local Universe.

**Acknowledgements.** We are grateful to the referee, A. Hirschauer, for his constructive comments. We thank Evan Skillman for useful comments. JV and CK acknowledge financial support from the Spanish MINECO grant PID2022-136598NB-C32 and from the AEI “Center of Excellence Severo Ochoa” award to the IAA (SEV-2017-0709).

This research used data obtained with the Dark Energy Spectroscopic Instrument (DESI). DESI construction and operations are managed by the Lawrence Berkeley National Laboratory. This material is based upon work supported by the U.S. Department of Energy, Office of Science, Office of High-Energy Physics, under Contract No. DE-AC02-05CH11231, and by the National Energy Research

Scientific Computing Center, a DOE Office of Science User Facility under the same contract. Additional support for DESI was provided by the U.S. National Science Foundation (NSF), Division of Astronomical Sciences under Contract No. AST-0950945 to the NSF’s National Optical-Infrared Astronomy Research Laboratory; the Science and Technology Facilities Council of the United Kingdom; the Gordon and Betty Moore Foundation; the Heising-Simons Foundation; the French Alternative Energies and Atomic Energy Commission (CEA); the National Council of Science and Technology of Mexico (CONACYT); the Ministry of Science and Innovation of Spain (MICINN), and by the DESI Member Institutions: [www.desi.lbl.gov/collaborating-institutions](http://www.desi.lbl.gov/collaborating-institutions).

## References

- Annikabi, F., La Torre, V., Tosi, M., et al. 2019, MNRAS, 482, 3892  
 Arellano-Córdova, K. Z., Berg, D. A., Mingozi, M., et al. 2024, arXiv e-prints, arXiv:2403.08401  
 Asari, N. V., Cid Fernandes, R., Stasińska, G., et al. 2007, MNRAS, 381, 263  
 Aver, E., Berg, D. A., Hirschauer, A. S., et al. 2022, MNRAS, 510, 373  
 Baldwin, J. A., Phillips, M. M., & Terlevich, R. 1981, PASP, 93, 5  
 Berg, D. A., Pogge, R. W., Skillman, E. D., et al. 2020, ApJ, 893, 96  
 Brinchmann, J., Charlot, S., White, S. D. M., et al. 2004, MNRAS, 351, 1151  
 Bruzual, G. & Charlot, S. 2003, MNRAS, 344, 1000  
 Cid Fernandes, R., Mateus, A., Sodré, L., Stasińska, G., & Gomes, J. M. 2005, MNRAS, 358, 363  
 Croxall, K. V., Pogge, R. W., Berg, D. A., Skillman, E. D., & Moustakas, J. 2016, ApJ, 830, 4  
 Denicoló, G., Terlevich, R., & Terlevich, E. 2002, MNRAS, 330, 69  
 DESI Collaboration, Adame, A. G., Aguilar, J., et al. 2023, arXiv e-prints, arXiv:2306.06308  
 Díaz, Á. I. & Zamora, S. 2022, MNRAS, 511, 4377  
 Dors, O. L., Pérez-Montero, E., Hägele, G. F., Cardaci, M. V., & Krabbe, A. C. 2016, MNRAS, 456, 4407  
 Esteban, C., Bresolin, F., Peimbert, M., et al. 2009, ApJ, 700, 654  
 Fitzpatrick, E. L. 1999, PASP, 111, 63  
 Fricke, K. J., Izotov, Y. I., Papaderos, P., Guseva, N. G., & Thuan, T. X. 2001, AJ, 121, 169  
 Garnett, D. R. 1992, AJ, 103, 1330  
 Garnett, D. R., Shields, G. A., Skillman, E. D., Sagan, S. P., & Dufour, R. J. 1997, ApJ, 489, 63  
 Gonzalez-Delgado, R. M., Perez, E., Tenorio-Tagle, G., et al. 1994, ApJ, 437, 239  
 Goswami, S., Silva, L., Bressan, A., et al. 2022, A&A, 663, A1  
 Goswami, S., Vilchez, J. M., Perez-Diaz, B., et al. 2024, arXiv e-prints, arXiv:2402.13240  
 Guseva, N. G., Izotov, Y. I., Papaderos, P., et al. 2001, A&A, 378, 756  
 Guseva, N. G., Izotov, Y. I., Stasińska, G., et al. 2011, A&A, 529, A149  
 Guseva, N. G., Izotov, Y. I., & Thuan, T. X. 2000, ApJ, 531, 776  
 Guseva, N. G., Papaderos, P., Izotov, Y. I., et al. 2003a, A&A, 407, 91  
 Guseva, N. G., Papaderos, P., Izotov, Y. I., et al. 2003b, A&A, 407, 105  
 Guseva, N. G., Papaderos, P., Izotov, Y. I., Noeske, K. G., & Fricke, K. J. 2004, A&A, 421, 519  
 Guseva, N. G., Papaderos, P., Meyer, H. T., Izotov, Y. I., & Fricke, K. J. 2009, A&A, 505, 63  
 Hägele, G. F., Díaz, Á. I., Terlevich, E., et al. 2008, MNRAS, 383, 209  
 Hägele, G. F., Pérez-Montero, E., Díaz, Á. I., Terlevich, E., & Terlevich, R. 2006, MNRAS, 372, 293  
 Haurberg, N. C., Salzer, J. J., Cannon, J. M., & Marshall, M. V. 2015, ApJ, 800, 121  
 Hirschauer, A. S., Salzer, J. J., Bresolin, F., Saviane, I., & Yegorova, I. 2015, AJ, 150, 71  
 Hirschauer, A. S., Salzer, J. J., Skillman, E. D., et al. 2016, ApJ, 822, 108  
 Hsyu, T., Cooke, R. J., Prochaska, J. X., & Bolte, M. 2017, ApJ, 845, L22  
 Izotov, Y. I., Chaffee, F. H., Foltz, C. B., et al. 1999, ApJ, 527, 757  
 Izotov, Y. I., Chaffee, F. H., & Green, R. F. 2001, ApJ, 562, 727  
 Izotov, Y. I., Guseva, N. G., Fricke, K. J., & Papaderos, P. 2009, A&A, 503, 61  
 Izotov, Y. I., Papaderos, P., Guseva, N. G., Fricke, K. J., & Thuan, T. X. 2004, A&A, 421, 539  
 Izotov, Y. I., Schaefer, D., Guseva, N. G., Thuan, T. X., & Worseck, G. 2024, MNRAS, 528, L10  
 Izotov, Y. I., Stasińska, G., Meynet, G., Guseva, N. G., & Thuan, T. X. 2006, A&A, 448, 955  
 Izotov, Y. I., & Thuan, T. X. 1998a, ApJ, 497, 227  
 Izotov, Y. I., & Thuan, T. X. 1998b, ApJ, 500, 188  
 Izotov, Y. I., & Thuan, T. X. 2004, ApJ, 602, 200  
 Izotov, Y. I., Thuan, T. X., & Guseva, N. G. 2012, A&A, 546, A122  
 Izotov, Y. I., Thuan, T. X., & Guseva, N. G. 2019, MNRAS, 483, 5491  
 Izotov, Y. I., Thuan, T. X., & Guseva, N. G. 2021, MNRAS, 504, 3996

- Izotov, Y. I., Thuan, T. X., Guseva, N. G., & Liss, S. E. 2018, MNRAS, 473, 1956
- Izotov, Y. I., Thuan, T. X., & Lipovetsky, V. A. 1994, ApJ, 435, 647
- Izotov, Y. I., Thuan, T. X., & Lipovetsky, V. A. 1997, ApJS, 108, 1
- Kauffmann, G., Heckman, T. M., Tremonti, C., et al. 2003, MNRAS, 346, 1055
- Kehrig, C., Telles, E., & Cuisinier, F. 2004, AJ, 128, 1141
- Kehrig, C., Vílchez, J. M., Pérez-Montero, E., et al. 2016, MNRAS, 459, 2992
- Kennicutt, Robert C., J. & Skillman, E. D. 2001, AJ, 121, 1461
- Kewley, L. J., Dopita, M. A., Sutherland, R. S., Heisler, C. A., & Trevena, J. 2001, ApJ, 556, 121
- Kniazev, A. Y., Pustilnik, S. A., Masegosa, J., et al. 2000, A&A, 357, 101
- Kojima, T., Ouchi, M., Rauch, M., et al. 2020, ApJ, 898, 142
- Kojima, T., Ouchi, M., Rauch, M., et al. 2021, ApJ, 913, 22
- Kumari, N., James, B. L., Irwin, M. J., Amorín, R., & Pérez-Montero, E. 2018, MNRAS, 476, 3793
- Kunth, D. & Östlin, G. 2000, A&A Rev., 10, 1
- Lara-López, M. A., Pilyugin, L. S., Zaragoza-Cardiel, J., et al. 2023, A&A, 669, A25
- Lee, H., Grebel, E. K., & Hodge, P. W. 2003, A&A, 401, 141
- Lee, H., Skillman, E. D., & Venn, K. A. 2005, ApJ, 620, 223
- Lee, J. C., Salzer, J. J., & Melbourne, J. 2004, ApJ, 616, 752
- Luridiana, V., Morisset, C., & Shaw, R. A. 2015, A&A, 573, A42
- Magrini, L. & Gonçalves, D. R. 2009, MNRAS, 398, 280
- Mateus, A., Sodré, L., Cid Fernandes, R., et al. 2006, MNRAS, 370, 721
- Melbourne, J., Phillips, A., Salzer, J. J., Gronwall, C., & Sarajedini, V. L. 2004, AJ, 127, 686
- Melnick, J., Heydari-Malayeri, M., & Leisy, P. 1992, A&A, 253, 16
- Nicholls, D. C., Dopita, M. A., Sutherland, R. S., et al. 2014, ApJ, 786, 155
- Pagel, B. E. J., Simonson, E. A., Terlevich, R. J., & Edmunds, M. G. 1992, MNRAS, 255, 325
- Peña, M., Stasińska, G., & Richer, M. G. 2007, A&A, 476, 745
- Pérez-Montero, E. 2017, PASP, 129, 043001
- Pérez-Montero, E., Vílchez, J. M., Cedrés, B., et al. 2011, A&A, 532, A141
- Pustilnik, S., Zasov, A., Kniazev, A., et al. 2003a, A&A, 400, 841
- Pustilnik, S. A., Engels, D., Kniazev, A. Y., et al. 2006, Astronomy Letters, 32, 228
- Pustilnik, S. A., Kniazev, A. Y., & Pramskij, A. G. 2005, A&A, 443, 91
- Pustilnik, S. A., Kniazev, A. Y., Pramskij, A. G., Ugrumov, A. V., & Masegosa, J. 2003b, A&A, 409, 917
- Pustilnik, S. A., Martin, J. M., Huchtmeier, W. K., et al. 2002, A&A, 389, 405
- Saviane, I., Ivanov, V. D., Held, E. V., et al. 2008, A&A, 487, 901
- Schaefer, A. L., Tremonti, C., Belfiore, F., et al. 2020, ApJ, 890, L3
- Skillman, E. D., Côté, S., & Miller, B. W. 2003, AJ, 125, 610
- Skillman, E. D. & Kennicutt, Robert C., J. 1993, ApJ, 411, 655
- Skillman, E. D., Salzer, J. J., Berg, D. A., et al. 2013, AJ, 146, 3
- Stanghellini, L., Magrini, L., Villaver, E., & Galli, D. 2010, A&A, 521, A3
- Takahashi, K., Yoshida, T., & Umeda, H. 2018, ApJ, 857, 111
- Terlevich, R., Melnick, J., Masegosa, J., Moles, M., & Copetti, M. V. F. 1991, A&AS, 91, 285
- Thuan, T. X., Guseva, N. G., & Izotov, Y. I. 2022, MNRAS, 516, L81
- Thuan, T. X., Izotov, Y. I., & Foltz, C. B. 1999, ApJ, 525, 105
- Thuan, T. X., Izotov, Y. I., & Lipovetsky, V. A. 1995, ApJ, 445, 108
- Toribio San Cipriano, L., Domínguez-Guzmán, G., Esteban, C., et al. 2017, MNRAS, 467, 3759
- van Zee, L. 2000, ApJ, 543, L31
- van Zee, L., Haynes, M. P., & Salzer, J. J. 1997, AJ, 114, 2479
- Vílchez, J. M. & Iglesias-Páramo, J. 2003, ApJS, 145, 225
- Vilchez, J. M. & Pagel, B. E. J. 1988, MNRAS, 231, 257
- Zinchenko, I. A. 2023, A&A, 674, L7
- Zinchenko, I. A. & Pilyugin, L. S. 2022, Astronomische Nachrichten, 343, e20220048
- Zinchenko, I. A., Pilyugin, L. S., Grebel, E. K., Sánchez, S. F., & Vílchez, J. M. 2016, MNRAS, 462, 2715
- Zinchenko, I. A., Vílchez, J. M., Pérez-Montero, E., et al. 2021, A&A, 655, A58
- Zou, H., Sui, J., Saintonge, A., et al. 2024, ApJ, 961, 173

## Appendix A: Comparison with the MPA/JHU catalog

To check the reliability of our measurements of the flux of emission lines in DESI galaxies, we performed a comparison of the emission line fluxes used in this work with the ones presented in the MPA/JHU catalog<sup>1</sup> for the SDSS (Brinchmann et al. 2004). From both catalogs we selected spectra with  $S/N > 3$  in  $[\text{O II}]\lambda\lambda 3727, 3729$ ,  $\text{H}\beta$ ,  $[\text{N II}]\lambda 6584$ ,  $[\text{O III}]\lambda 5007$ , and  $\text{H}\alpha$  lines. Then, we cross-matched their positions on the sky requiring the maximal difference in fiber positions of 0.3 arcsecond which is significantly smaller than the diameter of DESI and SDSS fibers. After applying these criteria, we found 5374 objects with emission line fluxes available in our DESI catalog and MPA/JHU catalog for SDSS galaxies.

In Fig. A.1 we compared the fluxes normalized by  $\text{H}\beta$  obtained from our catalog of DESI objects and the MPA/JHU catalog. It demonstrates that our measurements of the nebular emission lines  $[\text{O II}]\lambda\lambda 3727, 3729$ ,  $[\text{O III}]\lambda 5007$ ,  $[\text{N II}]\lambda 6584$ , needed for determination of the oxygen abundance and N/O ratio, are in a very good agreement with the ones from the MPA/JHU catalog.  $\text{H}\alpha/\text{H}\beta$  line ratio used for extinction correction also shows no systematic offset between our measurements and the MPA/JHU catalog.

## Appendix B: Emission line intensities

---

<sup>1</sup> [https://www.sdss4.org/dr17/spectro/galaxy\\_mpajhu/](https://www.sdss4.org/dr17/spectro/galaxy_mpajhu/)

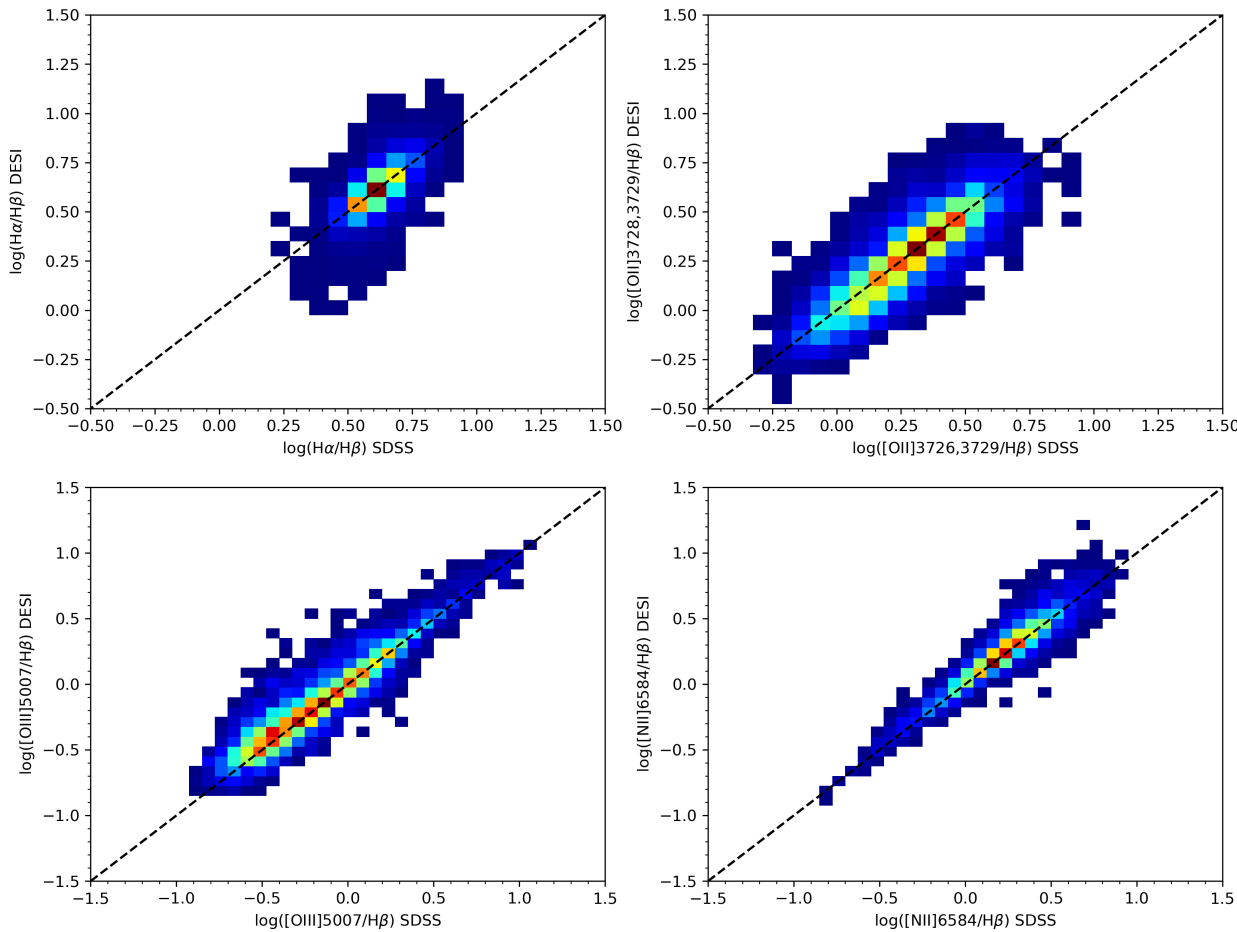


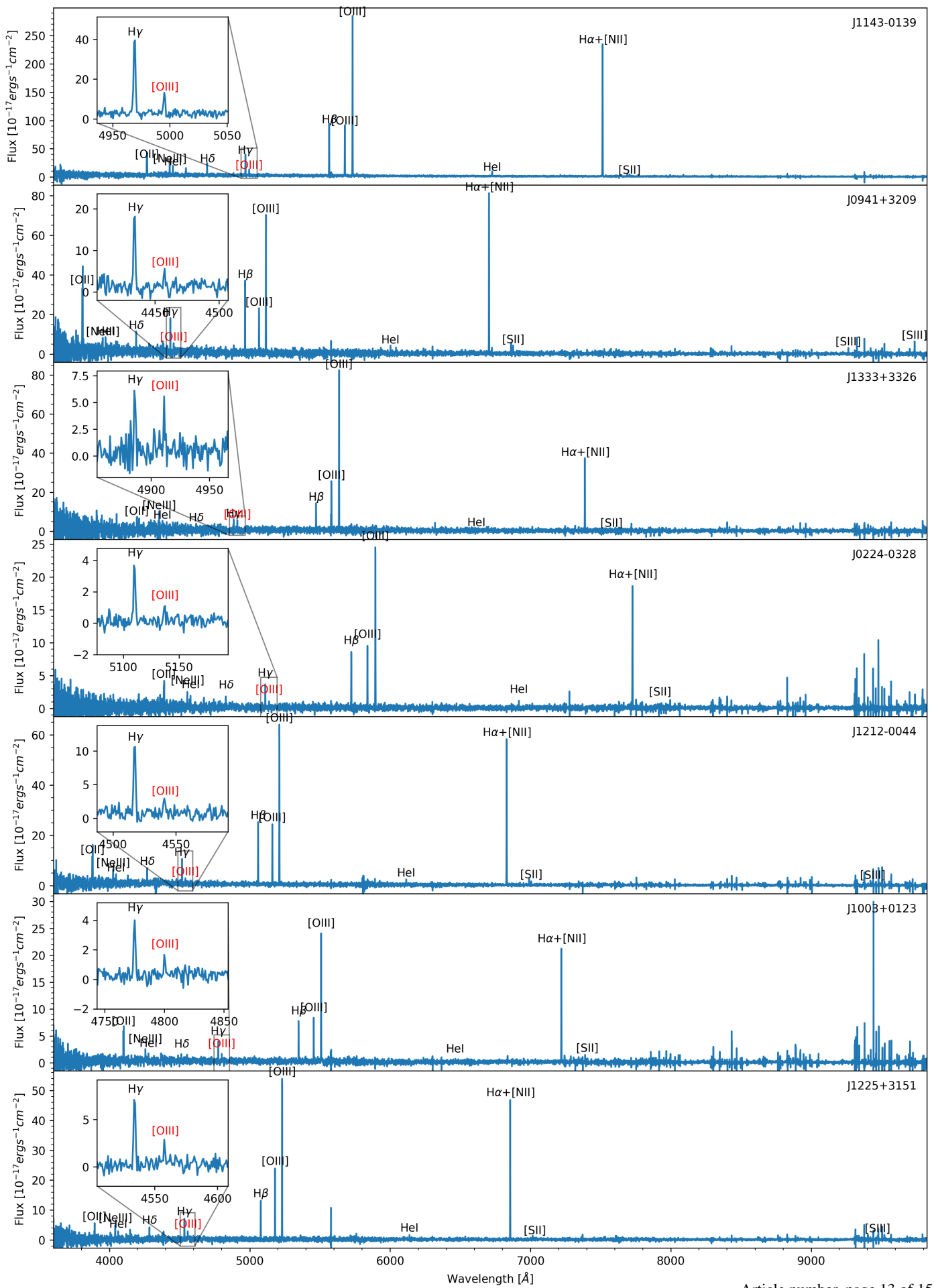
**Fig. A.1.** Comparison of the emission line fluxes measured by us for the DESI galaxies with the ones presented in the MPA/JHU catalog as a part of SDSS. 2D histograms show the number of objects in the flux bin. Only bins with 3 or more objects are shown. The dashed line shows one-to-one correspondence between fluxes.

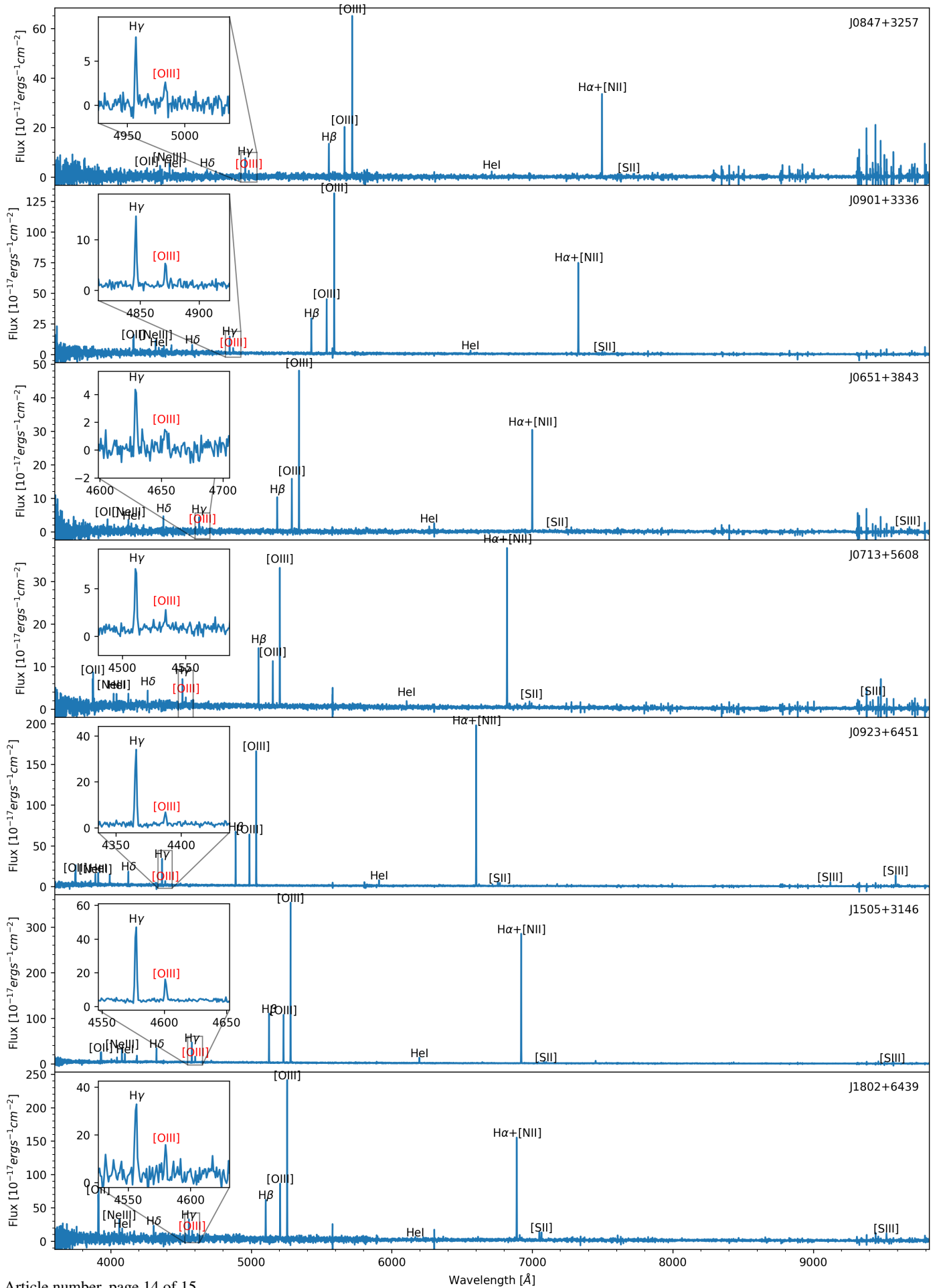
**Table B.1.** Emission line intensities before correction for extinction. Fluxes are in units of  $10^{-17}$  erg s $^{-1}$  cm $^{-2}$

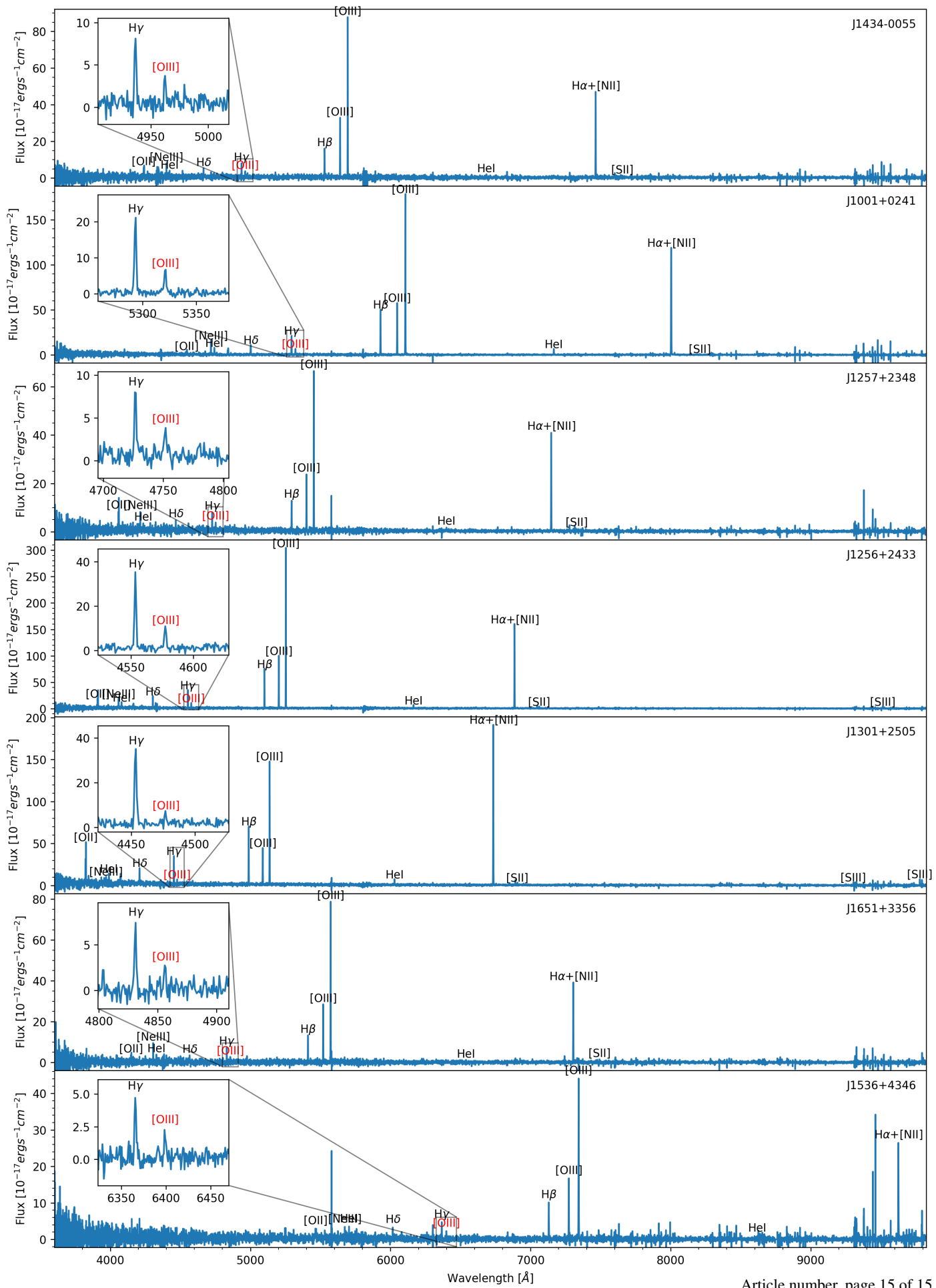
	J1143-0139	J0941+3209	J1333+3326	J0224-0328	J1212-0044	J1003+0123	J1225+3151	J0847+3257	J0901+3336	J0651+3843	J0713+5608
[O II] $\lambda$ 3726	58.11 $\pm$ 2.97	52.52 $\pm$ 4.89	8.13 $\pm$ 2.68	6.05 $\pm$ 0.92	20.74 $\pm$ 1.93	9.63 $\pm$ 0.75	3.81 $\pm$ 1.23	6.20 $\pm$ 1.64	18.95 $\pm$ 2.08	4.22 $\pm$ 1.17	10.85 $\pm$ 1.20
[O II] $\lambda$ 3729	76.68 $\pm$ 3.16	79.85 $\pm$ 5.07	14.33 $\pm$ 2.91	9.12 $\pm$ 0.97	28.57 $\pm$ 1.98	11.83 $\pm$ 0.77	9.76 $\pm$ 1.49	8.06 $\pm$ 1.73	29.92 $\pm$ 2.22	8.23 $\pm$ 1.33	15.10 $\pm$ 1.30
H9	—	—	—	—	5.76 $\pm$ 0.91	10.00 $\pm$ 1.53	3.85 $\pm$ 0.62	10.38 $\pm$ 1.15	10.45 $\pm$ 1.79	18.67 $\pm$ 2.04	6.62 $\pm$ 1.03
[Ne III] $\lambda$ 3869	44.47 $\pm$ 3.60	13.99 $\pm$ 3.91	—	—	3.01 $\pm$ 0.79	4.56 $\pm$ 1.39	2.18 $\pm$ 0.57	5.97 $\pm$ 1.09	—	7.50 $\pm$ 1.87	4.74 $\pm$ 0.84
[He I] $\lambda$ +H8	29.38 $\pm$ 3.01	18.07 $\pm$ 3.72	—	—	—	—	—	—	—	3.87 $\pm$ 0.89	5.61 $\pm$ 0.86
[Ne III] $\lambda$ 3967	14.17 $\pm$ 2.50	—	—	—	4.83 $\pm$ 1.09	5.38 $\pm$ 1.17	7.43 $\pm$ 1.83	4.12 $\pm$ 0.89	—	5.38 $\pm$ 1.51	2.14 $\pm$ 0.69
H $\epsilon$	28.53 $\pm$ 2.75	—	—	—	—	—	—	—	—	8.82 $\pm$ 1.56	4.93 $\pm$ 0.79
[He I] $\lambda$ 4027	—	—	—	—	—	—	—	—	—	—	—
[S III] $\lambda$ 4069	—	—	—	—	—	—	—	—	—	—	—
[S III] $\lambda$ 4076	—	—	—	—	—	—	—	—	—	—	—
H6	40.72 $\pm$ 2.68	18.87 $\pm$ 2.45	—	—	4.36 $\pm$ 0.65	13.11 $\pm$ 1.31	3.28 $\pm$ 0.73	6.74 $\pm$ 0.86	7.44 $\pm$ 1.42	14.44 $\pm$ 1.72	7.03 $\pm$ 1.35
H $\gamma$	80.34 $\pm$ 2.70	31.93 $\pm$ 2.02	9.41 $\pm$ 1.45	—	7.51 $\pm$ 0.53	20.87 $\pm$ 1.17	7.26 $\pm$ 0.53	13.64 $\pm$ 0.95	13.53 $\pm$ 1.08	23.47 $\pm$ 1.02	9.43 $\pm$ 0.89
[O III] $\lambda$ 4363	19.54 $\pm$ 1.87	6.40 $\pm$ 1.49	6.36 $\pm$ 1.31	1.90 $\pm$ 0.44	4.27 $\pm$ 0.95	2.22 $\pm$ 0.46	4.01 $\pm$ 0.77	4.79 $\pm$ 0.91	7.89 $\pm$ 0.69	3.21 $\pm$ 0.75	2.80 $\pm$ 0.61
[He I] $\lambda$ 4472	—	—	—	—	—	—	—	—	—	—	—
[Fe III] $\lambda$ 4658	—	—	—	—	—	—	—	—	—	—	—
[He II] $\lambda$ 4686	—	—	—	—	—	—	—	—	—	—	—
[He I] $\lambda$ 4714	—	—	—	—	—	—	—	—	—	—	—
[Ar IV] $\lambda$ 4741	—	—	—	—	—	—	—	—	—	—	—
H $\beta$	176.82 $\pm$ 3.75	61.29 $\pm$ 2.22	24.47 $\pm$ 1.78	16.88 $\pm$ 0.61	42.57 $\pm$ 1.01	12.99 $\pm$ 0.53	25.21 $\pm$ 0.90	29.50 $\pm$ 1.60	52.94 $\pm$ 1.25	18.87 $\pm$ 0.63	25.16 $\pm$ 0.58
[He I] $\lambda$ 4923	—	—	—	—	—	—	—	—	—	—	—
[O III] $\lambda$ 4959	184.29 $\pm$ 3.68	48.16 $\pm$ 2.14	48.87 $\pm$ 2.40	17.14 $\pm$ 0.54	40.49 $\pm$ 0.98	14.07 $\pm$ 0.54	35.54 $\pm$ 1.00	37.47 $\pm$ 1.83	70.33 $\pm$ 1.76	26.89 $\pm$ 0.75	20.56 $\pm$ 0.56
[O III] $\lambda$ 5007	518.41 $\pm$ 5.47	130.28 $\pm$ 2.68	122.22 $\pm$ 2.74	51.45 $\pm$ 0.76	111.45 $\pm$ 1.23	40.52 $\pm$ 0.72	96.33 $\pm$ 1.37	115.88 $\pm$ 2.91	194.56 $\pm$ 2.48	73.02 $\pm$ 0.94	54.15 $\pm$ 0.72
[He I] $\lambda$ 5017	—	—	—	—	—	—	—	—	—	—	—
[N II] $\lambda$ 5199	—	—	—	—	—	—	—	—	—	—	—
[N II] $\lambda$ 5201	—	—	—	—	—	—	—	—	—	—	—
[N II] $\lambda$ 5755	—	—	—	—	—	—	—	—	—	—	—
[He I] $\lambda$ 5875	20.50 $\pm$ 1.06	6.57 $\pm$ 1.33	—	—	3.89 $\pm$ 0.70	1.38 $\pm$ 0.40	2.53 $\pm$ 0.48	—	4.54 $\pm$ 0.48	2.12 $\pm$ 0.47	3.03 $\pm$ 0.45
[O I] $\lambda$ 6300	6.08 $\pm$ 0.97	—	—	—	—	—	—	—	3.13 $\pm$ 0.63	—	—
[S III] $\lambda$ 6312	—	—	—	—	—	—	—	—	—	—	—
[N II] $\lambda$ 6548	—	—	—	—	—	—	—	—	—	—	—
Ha	540.63 $\pm$ 4.39	167.81 $\pm$ 2.08	68.81 $\pm$ 1.73	43.97 $\pm$ 0.79	123.77 $\pm$ 1.23	38.01 $\pm$ 0.50	66.99 $\pm$ 0.92	70.85 $\pm$ 1.37	150.07 $\pm$ 1.51	53.85 $\pm$ 0.55	70.91 $\pm$ 0.69
[N II] $\lambda$ 6584	4.96 $\pm$ 1.08	4.55 $\pm$ 0.90	—	—	1.23 $\pm$ 0.39	—	—	—	—	0.75 $\pm$ 0.25	1.49 $\pm$ 0.32
[He I] $\lambda$ 6680	3.49 $\pm$ 0.92	—	—	—	1.53 $\pm$ 0.46	—	—	—	—	0.98 $\pm$ 0.28	ED—
[S III] $\lambda$ 6717	11.18 $\pm$ 0.89	12.09 $\pm$ 0.90	—	—	1.87 $\pm$ 0.44	4.54 $\pm$ 0.41	1.94 $\pm$ 0.30	1.42 $\pm$ 0.26	1.89 $\pm$ 0.49	3.97 $\pm$ 0.57	2.49 $\pm$ 0.37
[S III] $\lambda$ 6731	9.17 $\pm$ 0.81	7.13 $\pm$ 0.93	—	—	—	2.79 $\pm$ 0.38	—	0.82 $\pm$ 0.27	—	2.64 $\pm$ 0.51	1.03 $\pm$ 0.30
[He I] $\lambda$ 7067	9.50 $\pm$ 0.79	2.38 $\pm$ 0.79	—	—	—	1.22 $\pm$ 0.41	—	—	1.60 $\pm$ 0.49	—	1.81 $\pm$ 0.24
[Ar III] $\lambda$ 7136	3.96 $\pm$ 0.64	—	—	—	—	1.97 $\pm$ 0.42	—	1.28 $\pm$ 0.36	—	—	—
[O II] $\lambda$ 7320	2.82 $\pm$ 0.76	—	—	—	—	—	—	—	—	—	—
[O II] $\lambda$ 7330	2.47 $\pm$ 0.74	—	—	—	—	—	2.21 $\pm$ 0.55	—	—	—	—
[Ar III] $\lambda$ 7751	—	4.20 $\pm$ 0.51	—	—	—	—	—	2.62 $\pm$ 0.40	—	—	—
[S III] $\lambda$ 79068	—	13.01 $\pm$ 1.21	—	—	—	3.50 $\pm$ 0.57	—	—	—	1.92 $\pm$ 0.61	—
[S III] $\lambda$ 79530	—	—	—	—	—	—	—	—	—	—	—
Pa8	—	—	—	—	—	—	—	—	—	—	—
C(H $\beta$ )	0.132 $\pm$ 0.029	0.000 $\pm$ 0.047	0.028 $\pm$ 0.096	0.000 $\pm$ 0.050	0.069 $\pm$ 0.033	0.078 $\pm$ 0.054	0.000 $\pm$ 0.048	0.000 $\pm$ 0.072	0.038 $\pm$ 0.033	0.046 $\pm$ 0.043	0.000 $\pm$ 0.031
EW(H $\beta$ )	83.4 $\pm$ 1.8	51.3 $\pm$ 1.9	28.9 $\pm$ 2.1	83.1 $\pm$ 3.0	63.6 $\pm$ 1.5	41.1 $\pm$ 1.7	82.3 $\pm$ 3.0	94.2 $\pm$ 5.1	58.4 $\pm$ 1.4	80.1 $\pm$ 2.7	35.5 $\pm$ 0.8

Table B.1. Continued

	J0923+6451	J1505+3146	J1802+6439	J1434-0055	J1001+0241	J1257+2348	J1256+2433	J1301+2505	J1651+3356	J1536+4346
[O II] $\lambda$ 3726	26.24 $\pm$ 2.11	37.65 $\pm$ 2.70	140.75 $\pm$ 9.27	9.88 $\pm$ 1.67	5.76 $\pm$ 1.51	14.46 $\pm$ 1.61	34.83 $\pm$ 3.11	66.71 $\pm$ 4.99	5.47 $\pm$ 1.44	6.30 $\pm$ 1.34
[O II] $\lambda$ 3729	38.56 $\pm$ 2.31	43.83 $\pm$ 3.08	177.74 $\pm$ 10.77	12.54 $\pm$ 1.68	9.43 $\pm$ 1.62	19.21 $\pm$ 1.83	54.47 $\pm$ 4.06	97.03 $\pm$ 6.13	6.63 $\pm$ 1.46	6.76 $\pm$ 1.28
H9	8.53 $\pm$ 1.71	16.59 $\pm$ 1.71	—	—	8.09 $\pm$ 1.27	—	—	—	—	4.01 $\pm$ 1.17
[Ne III] $\lambda$ 3869	25.03 $\pm$ 1.67	50.29 $\pm$ 2.69	62.42 $\pm$ 7.56	12.83 $\pm$ 1.75	33.00 $\pm$ 1.65	13.16 $\pm$ 1.69	38.46 $\pm$ 3.25	18.73 $\pm$ 3.64	13.65 $\pm$ 1.42	5.35 $\pm$ 1.18
[He I] $\lambda$ H8	28.75 $\pm$ 1.74	30.82 $\pm$ 2.05	30.83 $\pm$ 6.66	4.48 $\pm$ 1.45	16.96 $\pm$ 1.32	4.64 $\pm$ 1.38	22.58 $\pm$ 2.66	26.93 $\pm$ 4.01	6.23 $\pm$ 1.21	5.23 $\pm$ 1.22
[Ne III] $\lambda$ 3967	6.51 $\pm$ 1.11	13.85 $\pm$ 1.43	15.10 $\pm$ 4.94	—	12.65 $\pm$ 1.16	4.03 $\pm$ 1.21	11.99 $\pm$ 2.42	12.96 $\pm$ 2.84	—	—
He $\epsilon$	20.66 $\pm$ 1.27	29.14 $\pm$ 1.89	17.56 $\pm$ 5.02	5.04 $\pm$ 1.38	17.72 $\pm$ 1.27	4.91 $\pm$ 1.28	16.65 $\pm$ 2.62	27.81 $\pm$ 3.14	—	6.00 $\pm$ 1.47
[He I] $\lambda$ 4027	—	—	—	—	—	—	—	—	—	—
[S II] $\lambda$ 4069	—	—	—	—	—	—	—	—	—	—
[S II] $\lambda$ 4076	—	—	—	—	—	—	—	—	—	—
H $\delta$	32.94 $\pm$ 1.36	47.34 $\pm$ 2.41	37.82 $\pm$ 5.23	8.78 $\pm$ 1.37	25.46 $\pm$ 1.35	7.01 $\pm$ 1.46	36.25 $\pm$ 2.90	38.76 $\pm$ 3.21	9.71 $\pm$ 2.34	7.94 $\pm$ 1.08
Hy	57.04 $\pm$ 1.58	83.74 $\pm$ 1.95	66.64 $\pm$ 6.02	15.43 $\pm$ 1.42	45.56 $\pm$ 1.53	15.81 $\pm$ 1.40	55.95 $\pm$ 2.59	64.74 $\pm$ 3.06	13.45 $\pm$ 1.45	10.80 $\pm$ 1.61
[O III] $\lambda$ 4363	8.62 $\pm$ 0.93	21.12 $\pm$ 1.17	22.69 $\pm$ 4.52	6.20 $\pm$ 1.13	14.67 $\pm$ 1.05	6.51 $\pm$ 1.14	17.20 $\pm$ 1.54	8.93 $\pm$ 1.79	5.30 $\pm$ 1.14	4.46 $\pm$ 0.79
[He I] $\lambda$ 4472	4.73 $\pm$ 0.93	5.21 $\pm$ 1.02	—	—	5.15 $\pm$ 1.31	—	11.99 $\pm$ 3.76	—	9.13 $\pm$ 2.70	—
[Fe III] $\lambda$ 4658	—	—	—	—	—	—	—	—	—	—
[He II] $\lambda$ 4686	—	3.20 $\pm$ 0.97	—	—	—	3.61 $\pm$ 1.13	—	—	—	—
[He I] $\lambda$ 4714	—	3.61 $\pm$ 1.00	—	—	—	—	—	—	—	2.09 $\pm$ 0.66
[Ar IV] $\lambda$ 4741	—	—	—	—	—	—	—	—	—	—
H $\beta$	114.35 $\pm$ 1.33	170.65 $\pm$ 2.78	134.53 $\pm$ 6.53	31.00 $\pm$ 1.57	104.89 $\pm$ 1.90	25.93 $\pm$ 1.38	108.09 $\pm$ 2.85	138.13 $\pm$ 3.40	26.63 $\pm$ 1.44	23.73 $\pm$ 1.17
[He I] $\lambda$ 4923	91.38 $\pm$ 1.25	166.94 $\pm$ 3.25	148.81 $\pm$ 6.01	48.79 $\pm$ 1.46	123.83 $\pm$ 2.14	44.44 $\pm$ 1.51	147.14 $\pm$ 3.62	81.76 $\pm$ 2.70	45.10 $\pm$ 1.90	35.11 $\pm$ 1.20
[O III] $\lambda$ 4959	255.55 $\pm$ 1.84	507.77 $\pm$ 5.48	427.48 $\pm$ 8.75	133.82 $\pm$ 2.12	366.54 $\pm$ 3.40	122.08 $\pm$ 2.10	418.97 $\pm$ 5.74	232.02 $\pm$ 4.09	125.46 $\pm$ 2.69	103.15 $\pm$ 2.94
[He I] $\lambda$ 5017	2.17 $\pm$ 0.56	—	—	—	2.84 $\pm$ 0.90	—	—	—	—	—
[N II] $\lambda$ 5199	—	—	—	—	—	—	—	—	—	—
[N II] $\lambda$ 5201	—	—	—	—	—	—	—	—	—	—
[N II] $\lambda$ 5755	—	—	—	—	—	—	—	—	—	—
[He I] $\lambda$ 5875	13.75 $\pm$ 0.69	21.58 $\pm$ 0.99	12.76 $\pm$ 2.53	4.75 $\pm$ 1.31	15.21 $\pm$ 0.69	—	—	11.88 $\pm$ 1.17	13.49 $\pm$ 1.25	—
[O I] $\lambda$ 6300	2.13 $\pm$ 0.36	2.45 $\pm$ 0.67	9.40 $\pm$ 2.15	—	—	—	—	2.94 $\pm$ 0.96	—	—
[S III] $\lambda$ 6312	1.53 $\pm$ 0.35	—	—	—	—	—	—	—	—	—
[N II] $\lambda$ 6548	—	—	—	—	—	—	—	—	—	—
Ha	340.29 $\pm$ 1.88	501.65 $\pm$ 4.78	278.06 $\pm$ 5.87	87.79 $\pm$ 1.50	322.69 $\pm$ 3.23	76.11 $\pm$ 1.15	319.44 $\pm$ 3.51	398.01 $\pm$ 4.49	82.27 $\pm$ 1.85	77.05 $\pm$ 3.80
[N II] $\lambda$ 6584	3.53 $\pm$ 0.52	—	14.07 $\pm$ 2.00	—	—	—	3.56 $\pm$ 0.85	—	—	—
[He I] $\lambda$ 6680	3.91 $\pm$ 0.36	5.49 $\pm$ 0.49	—	—	3.88 $\pm$ 0.54	—	2.92 $\pm$ 0.85	4.50 $\pm$ 0.75	—	—
[S II] $\lambda$ 6717	9.44 $\pm$ 0.40	7.27 $\pm$ 0.51	34.28 $\pm$ 2.28	—	1.66 $\pm$ 0.55	3.78 $\pm$ 0.52	11.69 $\pm$ 0.95	12.62 $\pm$ 1.12	—	—
[S II] $\lambda$ 6731	6.71 $\pm$ 0.32	4.81 $\pm$ 0.45	24.86 $\pm$ 1.94	—	1.94 $\pm$ 0.48	—	8.28 $\pm$ 0.84	7.03 $\pm$ 0.82	2.38 $\pm$ 0.47	—
[He I] $\lambda$ 7067	2.31 $\pm$ 0.27	11.90 $\pm$ 0.67	—	—	12.85 $\pm$ 1.04	—	3.27 $\pm$ 0.81	—	—	—
[Ar III] $\lambda$ 7136	4.34 $\pm$ 0.33	2.70 $\pm$ 0.65	6.30 $\pm$ 1.66	—	3.11 $\pm$ 0.62	0.98 $\pm$ 0.32	7.67 $\pm$ 1.30	4.64 $\pm$ 1.13	—	—
[O II] $\lambda$ 7320	—	—	3.65 $\pm$ 1.17	—	—	—	1.53 $\pm$ 0.48	3.17 $\pm$ 0.92	—	—
[O II] $\lambda$ 7330	—	—	—	—	—	—	—	—	—	—
[Ar III] $\lambda$ 7751	—	—	—	—	—	—	—	—	—	—
[S III] $\lambda$ 7908	9.02 $\pm$ 0.29	—	—	—	—	—	—	10.14 $\pm$ 0.82	8.58 $\pm$ 1.05	—
[S III] $\lambda$ 79530	24.90 $\pm$ 0.53	—	—	—	—	—	—	20.72 $\pm$ 1.31	—	—
Pa8	5.13 $\pm$ 0.32	—	—	—	—	—	—	—	—	—
C(H $\beta$ )	0.098 $\pm$ 0.017	0.083 $\pm$ 0.024	0.000 $\pm$ 0.066	0.037 $\pm$ 0.068	0.140 $\pm$ 0.026	0.081 $\pm$ 0.069	0.090 $\pm$ 0.035	0.058 $\pm$ 0.033	0.145 $\pm$ 0.075	0.207 $\pm$ 0.087
EW(H $\beta$ )	82.9 $\pm$ 1.0	62.2 $\pm$ 1.0	41.1 $\pm$ 2.0	51.6 $\pm$ 2.6	304.7 $\pm$ 5.6	40.2 $\pm$ 2.1	86.7 $\pm$ 4.0	90.0 $\pm$ 2.2	74.9 $\pm$ 4.0	104.4 $\pm$ 5.2

**Fig. B.1.** DESI spectra of our sample of galaxies. Selected emission lines are labelled.



**Fig. B.3.** DESI spectra of our sample of galaxies. Selected emission lines are labelled (continued).